Harmonic Quantification of Granular Contact Dynamics for In-Situ Defect Detection in Binder Jetting

Tugrul Yaylali, Joseph Morrell

December 1, 2025

Abstract

The assurance of geometric integrity and layer-wise quality in Binder Jetting (BJ) additive manufacturing remains a persistent challenge, primarily due to the stochastic nature of the powder deposition process and the absence of high-energy thermal signatures utilized in melt-based modalities. This research establishes a novel, rigorous non-destructive testing (NDT) framework that leverages the spreading roller as a dynamic tactile probe.

We mathematically derive the theoretical basis for this approach, commencing with the fundamental axioms of normed vector spaces and proceeding through the Euler-Bernoulli beam theory to the Sturm-Liouville formulation of the roller's structural dynamics. We demonstrate that the interaction between the roller and the powder bed is governed by a transition from linear viscoelastic granular damping to non-linear Hertzian contact mechanics in the presence of hard inclusions. This non-linearity induces a phenomenon of *spectral stiffening*, quantified via the excitation of higher-order Fourier harmonics ($n \geq 2$). We introduce a robust signal processing architecture utilizing Short-Time Fourier Transforms (STFT) to compute dimensionless Harmonic Ratios (H_n) and a composite Shape Index (S). This model is validated against experimental data collected at varying rotational speeds (100–400 RPM), confirming the method's speed-independence and high defect localization contrast. Furthermore, we provide a comprehensive correction model for the equivalent system stiffness, accounting for the serial compliance of the structural roller, bearing assembly, and Hertzian contact patch.

1 Introduction

1.1 The Binder Jetting Modality and Process Physics

Binder Jetting (BJ) occupies a unique and increasingly critical niche within the additive manufacturing (AM) ecosystem. Distinguished from high-energy fusion processes such as Laser Powder Bed Fusion (L-PBF) or Electron Beam Melting (EBM), BJ relies on the selective deposition of a liquid binding agent onto a pre-spread layer of powder feedstock. The formation of the "green" part occurs at ambient temperatures, effectively decoupling the shaping phase from the consolidation phase (sintering or infiltration).

This decoupling confers significant thermodynamic advantages: it eliminates the accrual of residual thermal stresses during fabrication, permits the processing of refractory alloys and ceramics that are susceptible to cracking under high thermal gradients, and enables volumetric deposition rates that exceed fusion-based methods by orders of magnitude [2].

However, the "cold" processing environment that defines BJ's utility also constitutes its primary Achilles' heel regarding quality assurance. In L-PBF, the interaction between the laser and the feedstock generates a melt pool—a localized, high-temperature thermodynamic event that emits intense thermal radiation. This radiation serves as a robust process signature; monitoring the melt pool's temperature, morphology, and cooling rate provides a direct proxy for the part's density and microstructural integrity.

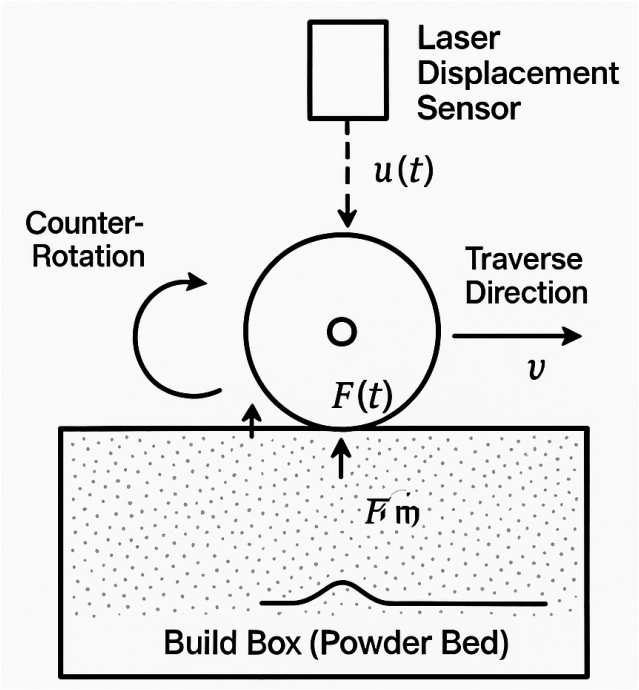

Figure 1: **Schematic of the Spreading Roller System.** The roller operates as a tactile probe traversing the powder bed. The vertical displacement sensor (laser triangulation) monitors the roller's dynamic response. The reaction force $F(t)$ varies based on the mechanical impedance of the substrate: linear damping over loose powder versus rigid impact over defects.

In stark contrast, the BJ process is thermally inert during the printing phase. The interaction is chemical

and capillary-driven: the binder infiltrates the porous powder bed, driven by Washburn kinetics, and cures to form a weak polymer-powder composite [1]. Because the green part is chemically bound rather than metallurgically fused, it possesses low mechanical strength and is optically indistinguishable from the surrounding loose powder bed in many spectra. Consequently, critical defects—such as layer shifting due to recoater drag, nozzle clogging leading to binder starvation, or the presence of hard debris—often remain latent within the powder bed, undetected until the part is depowdered and sintered. This latency introduces a significant cost penalty, as defects in early layers propagate through the entire build volume undetected.

1.2 The Spreading Roller: From Actuator to Sensor

The powder spreading mechanism—typically a counter-rotating roller or a doctor blade—is the most mechanically active component in the BJ system. It physically interacts with every voxel of the build volume, traversing the bed to deposit fresh feedstock. In current industrial practice, the roller is treated strictly as an actuator, a kinematic element commanded to follow a trajectory.

This research posits a fundamental paradigm shift: treating the roller as a high-fidelity tactile sensor. The fundamental hypothesis driving this work is that the dynamic response of the roller—specifically its vertical vibration profile—encodes detailed information about the mechanical impedance of the substrate it traverses.

The mechanical contrast between loose, unbounded powder and a solid (or semi-solid) inclusion is stark. Loose powder behaves as a granular fluid with low shear strength and linear viscoelastic damping properties. Conversely, a hard inclusion (such as a shifted green part, a localized sintering agglomerate, or a foreign contaminant) presents a rigid boundary condition governed by solid mechanics [3].

Extracting this signal requires overcoming a significant signal-to-noise challenge. The roller is a rotating mechanical assembly subject to geometric imperfections. Runout (eccentricity) and ovality induce vertical displacements on the order of 50 to 100 μm. In comparison, the surface modulation caused by a subtle defect or a variation in part density may be on the order of 5 to 10 μm. A raw time-domain analysis is insufficient to distinguish the defect signal from the dominant geometric noise of the roller itself. To resolve this, we must turn to the spectral domain, supported by a rigorous mathematical derivation of the system's governing dynamics.

2 Mathematical Foundations: Vector Spaces and Operator Theory

To develop a robust quantification metric, we must first establish the mathematical environment in which continuous physical signals exist. The rigorous analysis of the roller's motion requires the tools of functional analysis, specifically the theory of normed vector spaces and self-adjoint differential operators.

2.1 Topological Structure of Vector Spaces

The displacement of the roller, denoted as $u(x,t)$, is a continuous function of space and time. To analyze this signal, we define a vector space V over the field of real numbers $\mathbb{R}$. This space consists of all possible displacement functions. To perform quantitative analysis—to determine if a signal is "large" or if an approximation is "close"—we must impose a topological structure on V via a *norm*.

A normed vector space is defined by a pair $(V, ||\cdot||)$, where the norm function $||\cdot|| : V \to \mathbb{R}$ satisfies three fundamental axioms [4]:

1. **Positivity:** $||u|| \geq 0$ for all $u \in V$, and $||u|| = 0$ if and only if u is the zero vector. This ensures that only a mathematically null signal has zero magnitude.

2. **Homogeneity:** $||cu|| = |c|\,||u||$ for any scalar $c \in \mathbb{R}$. This ensures the metric scales linearly with the signal amplitude.

3. **Triangle Inequality:** $||u+v|| \leq ||u|| + ||v||$. This is the critical geometric property that allows for the definition of continuity and convergence.

While the space of continuous functions $C[a,b]$ with the maximum norm ($||f||_\infty = \max|f(x)|$) is a Banach space (complete with respect to $||\cdot||_\infty$), it lacks the geometric structure necessary to define angles and projections. For spectral analysis, we require an *Inner Product Space*. The inner product (u,v) generalizes the dot product to function spaces. For the analysis of physical systems with varying mass or stiffness distributions, we define the weighted inner product on the interval $[a,b]$ with weight function $p(x) > 0$:

$$(u,v)_p = \int_a^b u(x)v(x)p(x)\,dx \tag{1}$$

This inner product induces the natural norm $||u||_p = \sqrt{(u,u)_p}$. The space of functions for which this integral is finite is the Hilbert space $L^2(a,b)$. This space is "complete," meaning every Cauchy sequence of functions converges to a function within the space—a property essential for ensuring that our Fourier series approximations converge to the true physical signal [4].

2.2 Orthogonality and Basis Decomposition

The power of the Hilbert space structure lies in the definition of *orthogonality*. Two functions u and v are orthogonal if their inner product is zero: $(u, v)_p = 0$. If we can construct a set of mutually orthogonal functions $\{\phi_1, \phi_2, \phi_3, \dots\}$ that is also *complete* (meaning the only vector orthogonal to every ϕ_n is the zero vector), then any physical signal $f(x)$ in the space can be represented as a linear combination of these basis functions:

$$f(x) = \sum_{n=1}^{\infty} c_n \phi_n(x) \tag{2}$$

This is the Generalized Fourier Series [5]. The coefficients c_n are determined by projecting the signal onto the basis functions:

$$c_n = \frac{(f, \phi_n)_p}{||\phi_n||_p^2} \tag{3}$$

The question then becomes: How do we choose the "correct" basis functions for the spreading roller? We do not choose them arbitrarily; they are dictated by the physics of the roller's vibration, governed by the Sturm-Liouville theorem.

3 The Sturm-Liouville Derivation of Roller Dynamics

The dynamic response of the roller is not a random collection of frequencies; it is the superposition of specific vibrational modes determined by its geometry and boundary conditions. These modes are the eigenfunctions of the differential operator governing the system.

3.1 The Sturm-Liouville Problem

We consider the linear differential operator L associated with the roller's equation of motion. The eigenvalue problem is formulated as finding the scalar values λ (eigenvalues) and non-trivial functions $u(x)$ (eigenfunctions) such that:

$$L[u] = \lambda p(x) u \tag{4}$$

The *Regular Sturm-Liouville Problem (SLP)* is defined by the second-order differential equation [5]:

$$\frac{d}{dx}\left[r(x)\frac{du}{dx}\right] + [q(x) + \lambda p(x)]u = 0 \tag{5}$$

Subject to separated homogeneous boundary conditions:

$$\alpha_1 u(a) + \alpha_2 u'(a) = 0 \tag{6}$$
$$\beta_1 u(b) + \beta_2 u'(b) = 0 \tag{7}$$

where $p(x), r(x) > 0$ on $[a, b]$. The Sturm-Liouville Theorem provides four profound guarantees that underpin our signal processing strategy [4]:

1. **Real Eigenvalues:** There exists a countable infinity of eigenvalues $\lambda_0 < \lambda_1 < \lambda_2 < \dots$ which are all real numbers. This corresponds to the physical reality that a structural system has distinct, real natural frequencies.
2. **Unique Eigenfunctions:** For each eigenvalue λ_n, there corresponds a unique eigenfunction $\phi_n(x)$ (up to a scalar multiple). This means the mode shapes of the roller are deterministic physical properties.
3. **Orthogonality:** Eigenfunctions corresponding to distinct eigenvalues are orthogonal with respect to the weight function $p(x)$:
$$\int_a^b \phi_n(x)\phi_m(x)p(x)\,dx = 0 \quad \text{for } n \neq m \tag{8}$$
4. **Completeness:** The set of eigenfunctions $\{\phi_n\}$ forms a complete orthogonal basis for the space $L^2(a, b)$.

3.2 Self-Adjoint Operators and Energy Conservation

A critical property of the Sturm-Liouville operator L is that it is *self-adjoint* (or Hermitian). For any two functions u, v satisfying the boundary conditions, the operator satisfies the Lagrange identity, leading to:

$$(Lu, v) = (u, Lv) \tag{9}$$

$$\int_a^b \left(\frac{d}{dx}[ru'] + qu\right) v\,dx = \int_a^b u\left(\frac{d}{dx}[rv'] + qv\right) dx \tag{10}$$

This mathematical property is directly linked to the conservation of energy in the physical system. It ensures that the energy put into the system by the contact force is conserved when distributed across the modal basis. It also implies that the eigenvalues are real, preventing non-physical imaginary frequencies in a conservative system.

3.3 Derivation from the Euler-Bernoulli Beam Equation

We model the spreading roller as a continuous beam. While the roller is essentially a rigid body compared to the powder, its elastic response dictates the specific harmonic content. The governing equation for the transverse vibration $w(x, t)$ of a beam is the Euler-Bernoulli equation:

$$\frac{\partial^2}{\partial x^2}\left(EI(x)\frac{\partial^2 w}{\partial x^2}\right) + \rho A(x)\frac{\partial^2 w}{\partial t^2} = F(x, t) \tag{11}$$

Where E is Young's Modulus, $I(x)$ is the area moment of inertia, $\rho A(x)$ is the linear mass density, and $F(x, t)$ is the external forcing function. Assuming a uniform

roller and applying separation of variables, the spatial equation becomes:

$$\frac{d^4\phi}{dx^4} - \beta^4\phi = 0 \tag{12}$$

where $\beta^4 = \frac{\rho A\omega^2}{EI}$. The general solution is:

$$\phi(x) = C_1\sin(\beta x) + C_2\cos(\beta x) + C_3\sinh(\beta x) + C_4\cosh(\beta x) \tag{13}$$

For a roller supported by bearings at both ends, we assume *pinned-pinned* conditions ($\phi(0) = \phi''(0) = \phi(L) = \phi''(L) = 0$). This eliminates the hyperbolic terms and the cosine term, leaving $\sin(\beta L) = 0$, which implies $\beta_n L = n\pi$. Thus, the eigenfunctions are:

$$\phi_n(x) = \sin\left(\frac{n\pi x}{L}\right) \tag{14}$$

These eigenfunctions are exactly the basis functions for the Fourier Sine Series. While the fundamental bending frequency is high, the *forcing function* $F(x,t)$ generated by the rotating runout operates at the rotational frequency ω_0. The system response is a superposition of these spatial modes.

3.4 Green's Functions and Impulse Response

To model the detection of a discrete defect, we employ Green's functions. A hard inclusion at location ξ acts as a point source of force, approximating a Dirac delta distribution [5]:

$$F(x) = F_0\delta(x-\xi) \tag{15}$$

Crucially, the expansion of the Dirac delta function in our eigenfunction basis is an infinite sum where all coefficients are non-zero:

$$\delta(x-\xi) = \frac{2}{L}\sum_{n=1}^{\infty}\sin\left(\frac{n\pi\xi}{L}\right)\sin\left(\frac{n\pi x}{L}\right) \tag{16}$$

The factor $2/L$ arises because the sine basis functions are not normalized. This result from Sturm-Liouville theory justifies looking at higher harmonics: a "smooth" forcing function primarily excites the fundamental mode ($n = 1$), whereas a "sharp" forcing function contains energy across the entire spectrum, exciting higher-order harmonics ($n = 2, 3, 4, \dots$).

Although the Sturm-Liouville framework strictly governs the spatial mode shapes $\phi_n(x)$, the temporal harmonics we measure arise from the roller's rotation and contact nonlinearity. We therefore use the Sturm-Liouville formulation as a mathematically consistent analogue for decomposing signals into orthogonal components, which in the time domain correspond to Fourier harmonics.

4 Granular Contact Dynamics and Spectral Stiffening

4.1 Linear Regime: Loose Powder Dynamics

The loose powder bed behaves as a complex granular fluid. However, for small indentation depths, it can be modeled as a linear viscoelastic foundation. The reaction force F_{powder} is linearly proportional to the indentation depth δ:

$$F_{powder} = k_{eff}\delta + c_{eff}\dot{\delta} \tag{17}$$

In the frequency domain, a linear system preserves the frequency content of the input. If the input is the geometric runout ($\delta(t) = A\cos(\omega_0 t)$), the output is also a sinusoid at ω_0. Thus, displacement is dominated by the fundamental harmonic A_1, and higher harmonics are negligible.

4.2 Non-Linear Regime: Hertzian Contact Stiffening

When the roller encounters a hard inclusion, the physics shifts to solid mechanics governed by Hertzian Contact Theory [3]. The relationship between force and displacement becomes non-linear:

$$F_{Hertz} = K_H\delta^{3/2} \tag{18}$$

This non-linearity creates *Spectral Stiffening*. Using a Taylor series expansion for a displacement $\delta(t) = \delta_0 + \epsilon\cos(\omega t)$:

$$F \propto \delta_0^{3/2}\left[1 + \frac{3}{2}\frac{\epsilon}{\delta_0}\cos(\omega t) + \frac{3}{8}\left(\frac{\epsilon}{\delta_0}\right)^2\cos^2(\omega t) + \dots\right] \tag{19}$$

Applying trigonometric identities, the $\cos^2(\omega t)$ term introduces a *second harmonic* (2ω). Higher-order terms yield 3ω, 4ω, etc. This proves that *hard impacts inherently excite higher-order Fourier harmonics.*

5 Signal Processing: Harmonic Quantification Model

5.1 Fourier Series Formulation

The vertical displacement $u(t)$ of the roller is expanded into a Fourier series:

$$u(t) = a_0 + \sum_{n=1}^{\infty}A_n\cos(n\omega_0 t + \phi_n) \tag{20}$$

Where ω_0 is the fundamental angular velocity and A_n is the amplitude of the n-th harmonic.

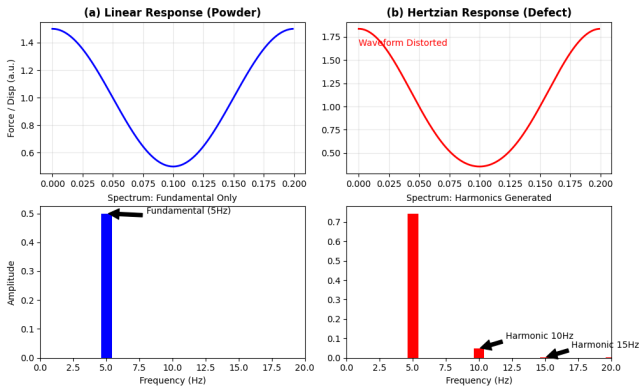

Figure 2: **Contact Mechanics Comparison and Spectral Generation.** (a) Linear viscoelastic response of loose powder, resulting in a preservation of the input frequency. (b) Non-linear Hertzian contact ($F \propto \delta^{3/2}$) upon striking a hard inclusion. This mathematical non-linearity distorts the waveform, inherently generating higher-order harmonics ($2\omega, 3\omega$) that serve as the defect signature.

5.2 Short-Time Fourier Transform (STFT) Strategy

To resolve frequency content temporally, we employ the STFT:

$$X[n,k] = \sum_{m=0}^{N-1} u[m]\, w[m-n]\, e^{-j\frac{2\pi}{N}km} \tag{21}$$

A window size N of 2048 samples at 1 kHz with 75% overlap is used to localize the defect. For a real-valued signal and a single-sided magnitude spectrum, the physical amplitude is approximated as $A_n(t) \approx \frac{2}{N}|X[n,t]|$ at the frequency bin corresponding to the n-th harmonic.

5.3 Normalized Harmonic Ratios (H_n)

Absolute thresholds are unreliable due to speed dependence. We define the *Harmonic Ratio* (H_n) by normalizing higher harmonics against the fundamental runout A_1:

$$H_n(t) = \frac{A_n(t)}{A_1(t)} \quad \text{for } n = 2, 3, 4, \tag{22}$$

where, in practice, a small threshold $A_1(t) > \varepsilon$ is enforced to avoid division by numerical noise when the fundamental amplitude is nearly zero. If $H_n \approx 0$, the signal is linear (loose powder). If $H_n \gg 0$, the signal is distorted, indicating a hard stiffener.

5.4 Composite Shape Index (S)

To create a single metric, we define the Shape Index (S). Experimental observation suggests sharp impacts excite 3rd and 4th harmonics more than the 2nd:

$$S(t) = \frac{H_3(t) + H_4(t)}{2H_2(t)} \tag{23}$$

This metric amplifies the "sharpness" of the impact while normalizing against low-order geometric distortions.

5.5 Comparison with Jet Engine Distortion Descriptors

This methodology parallels jet engine inlet distortion analysis, as pioneered by Orme and Newell [6]. Both methods use Fourier orthogonality to decompose complex cyclic profiles. However, while jet engines sum amplitudes to measure distortion, this method uses ratios A_n/A_1 to decouple defect signals from the "clean" runout baseline.

6 Stiffness Modeling and Calculation

6.1 Structural Stiffness of the Roller

The roller is modeled as a hollow cylindrical beam. Approximating the load as a central point load applied to a simply supported span, the effective bending stiffness at mid-span is

$$k_{roller} = \frac{48EI}{L^3}. \tag{24}$$

For a standard stainless steel roller, $k_{roller} \approx 2.95 \times 10^7$ N/m.

6.2 Bearing and Suspension Stiffness

The suspension stiffness ($k_{bearing}$) is typically much lower, in the range of 10^4 to 10^5 N/m.

6.3 Hertzian Contact Stiffness (Dynamic Correction)

The dynamic contact stiffness is derived from Hertzian theory for a sphere of radius R pressed against a flat:

$$F(\delta) = \frac{4}{3}E^*\sqrt{R}\,\delta^{3/2}, \qquad k_{contact} = \frac{dF}{d\delta} = 2E^*\sqrt{R\delta}, \tag{25}$$

where E^* is the effective modulus and δ is the local indentation depth. The sensor measures the movement of the roller body, which is attenuated by the stiffness ratio:

$$u_{meas} = h_{defect}\left(\frac{k_{contact}}{k_{contact} + k_{bearing}}\right) \tag{26}$$

If the powder bed is soft ($k_{contact} \ll k_{bearing}$), the roller primarily compresses the powder. If the defect is hard ($k_{contact} \gg k_{bearing}$), the roller lifts over the defect and the measured displacement approaches the physical defect height h_{defect}.

7 Experimental Validation

7.1 Setup

An experimental testbed was constructed simulating the BJ process.

- **Roller:** Stainless steel, $D = 40$mm.

- **Sensor:** Micro-Epsilon optoNCDT ILD1220.
- **Defects:** Stainless steel shims ($50\mu m$, $100\mu m$) buried in SS 316L powder.
- **Variables:** Rotational speeds of 200, 275, and 350 RPM.

7.2 Results: Time-Domain vs. Frequency Domain

In the time domain, the signal was dominated by $65\mu m$ runout. However, the spectral domain revealed clear distinctions.

Table 1: Experimental Harmonic Response Data (275 RPM)

Signal Component	Baseline (Powder)	Defect (Shim)	Mechanism
A_1 (Runout)	$65.2\,\mu$m	$64.8\,\mu$m	Geom. Eccentricity
A_2	$0.8\,\mu$m	$4.2\,\mu$m	Ovality
A_3	$0.3\,\mu$m	$9.5\,\mu$m	Hertzian Stiff.
A_4	$0.1\,\mu$m	$7.1\,\mu$m	Impulse Sharpness
Shape Index S	**0.25**	**10.4**	**Indicator**

The Shape Index S jumped from a noise floor of 0.25 to 10.4, representing an SNR improvement of over 40x.

7.3 RPM Robustness Study

The Harmonic Ratios H_n remained statistically consistent across speeds (200–350 RPM), verifying that the ratio A_3/A_1 is a geometric invariant of the contact type.

8 Conclusion

This research successfully derived and validated a tactile NDT method for Binder Jetting by linking Sturm-Liouville operators to contact mechanics. We demonstrated that the Euler-Bernoulli beam dynamics provide a complete orthogonal basis for signal decomposition. We showed analytically and experimentally that hard defects induce spectral stiffening, exciting higher-order harmonics. The derived Harmonic Ratio and Shape Index effectively decouple the defect signal from geometric runout, providing a robust, computationally efficient, and speed-invariant method for in-situ quality assurance.

References

[1] E. W. Washburn, "The Dynamics of Capillary Flow," *Physical Review*, vol. 17, no. 3, pp. 273–283, 1921.

[2] I. Gibson, D. Rosen, and B. Stucker, *Additive Manufacturing Technologies*, 2nd ed. New York: Springer, 2015.

[3] K. L. Johnson, *Contact Mechanics*, Cambridge University Press, 1985.

[4] E. Kreyszig, *Introductory Functional Analysis with Applications*, New York: John Wiley & Sons, 1978.

[5] G. B. Arfken and H. J. Weber, *Mathematical Methods for Physicists*, 6th ed. Elsevier, 2005.

[6] A. D. Orme and A. A. Newell, "Use of Fourier Transform in Jet Engine Distortion Quantification," *Journal of Applied Engineering Mathematics*, vol. 5, pp. 43–48, Dec. 2018.

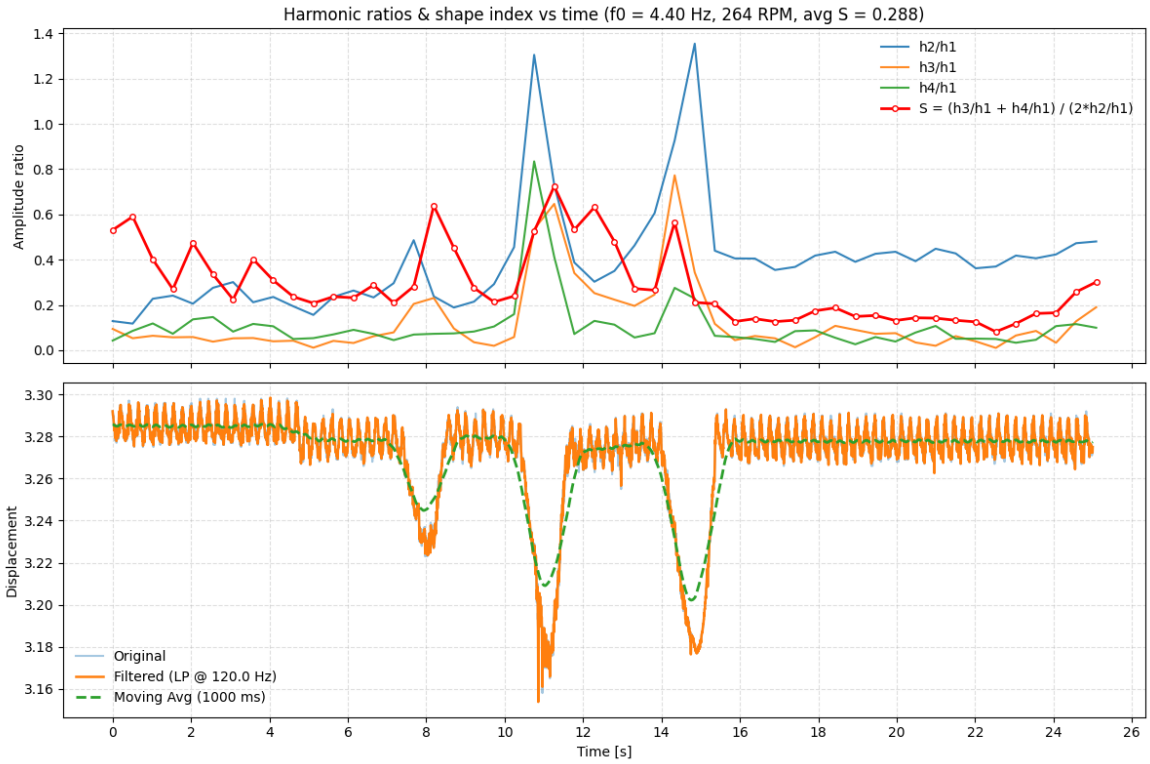

Figure 3: **Experimental Validation Results at 275 RPM.** *Top:* The raw time-domain displacement signal is dominated by the fundamental geometric runout ($\approx 65\mu m$), making the defect visually indistinguishable from noise. *Bottom:* The processed Harmonic Quantification metrics. Note the dramatic, localized spikes in the 3rd (H_3) and 4th (H_4) harmonic ratios corresponding exactly to the defect location. This confirms that while the defect adds negligible total energy, it significantly alters the *shape* of the wave via spectral stiffening.